Computers and Electronics in Agriculture 226 (2024) 109443

Contents lists available at ScienceDirect

Computers and Electronics in Agriculture

journal homepage: www.elsevier.com/locate/compag

The RapidMapper: State-of-the-art in mobile proximal soil sensing based on a novel multi-sensor platform

Hamed Tavakoli [a,*], José Correa [a], Sebastian Vogel [a], Marcel Oertel [a], Marc Zimne [a], Michael Heisig [a], Anatolij Harder [a], Robert Wruck [a], Stefan Pätzold [b], Matthias Leenen [b,c], Robin Gebbers [a,d]

[a] Department of Agromechatronics, Leibniz Institute for Agricultural Engineering and Bioeconomy e.V. (ATB), Max-Eyth-Allee 100, 14469 Potsdam, Germany
[b] University of Bonn, Institute for Crop Science and Resource Conservation (INRES) - Soil Science and Soil Ecology, Nussallee 13, 53115 Bonn, Germany
[c] Federal Office for Agriculture and Food, Deichmanns Aue 29, 53179 Bonn, Germany
[d] Martin Luther University Halle-Wittenberg, Chair of Agricultural Business Operations, Karl-Freiherr-von-Fritsch-Straße 4, 06120 Halle, Germany

ARTICLE INFO

Keywords:
Proximal soil sensing
Soil fertility
Sensor data quality assessment
NIR spectroscopy
Gamma-ray spectrometry

ABSTRACT

A rapid, accurate and high-resolution characterization of soil properties is essential for a successful implementation of site-specific soil and crop management in precision agriculture. In recent years, proximal soil sensors have been developed as efficient tools for high-resolution soil mapping. Nevertheless, no single soil sensor is capable of accurately quantifying all agronomically relevant soil properties. By integrating multiple proximal sensing technologies in a single multi-sensor platform, measuring simultaneously and fusing the sensor data by applying state-of-the-art machine learning algorithms, a greater variety of soil properties can be determined and the performance of soil property estimations can be improved. To this end, a multi-sensor platform for on-the-go topsoil mapping called RapidMapper was developed. Currently, it integrates near infrared and gamma-ray spectroscopy, apparent electrical conductivity and pH potentiometry (ion-selective electrode) sensors. We evaluated RapidMapper's functionality across various plots and fields in different regions of Germany. This paper focuses on data quality assessment for one multi-plot sensor test site and one agricultural field in northeast Germany. This includes analyzing sensor response across different soils, evaluating measurement consistency over three years on the same field and comparing data with other platforms and against laboratory measurements. The evaluation demonstrated RapidMapper's consistent mapping capabilities, high temporal consistency and strong agreement with similar devices.

1. Introduction

Soil is the key resource for crop production in agriculture. It is spatially and temporally variable within a field, as reflected through its soil properties. Characterization of the within-field soil variability is fundamental for a successful implementation of site-specific soil and crop management in precision agriculture, which aims to optimize plant production (Gebbers and Adamchuk, 2010; Hummel et al., 1996; Kuang et al., 2012).

The traditional method for quantifying soil variability is through soil sampling and laboratory analyses. However, the high costs involved result in low sampling densities, which limits an accurate quantification. Alternatively, various proximal soil sensors have been developed for measurement of soil properties at high spatial resolution, rapidly and cost-effectively on site (Adamchuk and Viscarra Rossel, 2010; Gebbers, 2018; Ji et al., 2019; Munnaf et al., 2020; Viscarra Rossel et al., 2011).

Gebbers (2018) classifies currently discussed proximal soil sensors into the following main groups:

a) Electrical sensors: They estimate soil apparent electrical resistivity (ER_a) / conductivity (ECa), or capacitance, which can be related to soil properties such as soil texture, organic matter content (SOM) / organic carbon content (SOC), moisture content (MC), salinity and/or pH.
b) Optical sensors: They assess the interaction between electromagnetic waves in wavelength ranges from 350 to 25000 nm, and soil constituents. These sensors include visible (Vis-), near infrared (NIR-) and mid-infrared (MIR) diffuse reflectance, laser-induced breakdown

* Corresponding author.
E-mail address: htavakoli@atb-potsdam.de (H. Tavakoli).

https://doi.org/10.1016/j.compag.2024.109443
Received 6 September 2023; Received in revised form 1 August 2024; Accepted 9 September 2024
Available online 22 September 2024

spectroscopy (LIBS) and Raman spectroscopy. Soil texture, SOM/SOC, cation exchange capacity (CEC), MC, pH, contamination by heavy metals and nutrients can affect this interaction.

c) Mechanical sensors: They measure either the forces required for dragging or pushing a tool through the soil, or the change in the level of noise caused by interaction between a tool and soil (acoustic sensors), or soil-air permeability (pneumatic sensors). These approaches can be applied for soil texture, mechanical resistance, and soil compaction determination.

d) Electrochemical sensors: They detect the activity of specific ions (e.g., H^+, NO_3^-, K^+, Na^+, Ca^{2+}, etc.) by means of either ion-selective electrodes (ISE), or ion-selective field effect transistors (ISFET). These sensors can be used for determining soil chemical properties such as nutrient contents or pH.

e) Thermal sensors: They measure either absolute or relative temperature of soil.

f) Radiometric sensors: They use radioactive radiation (gamma, alpha, beta, neutron radiation) (Knödel et al., 2005). Active radiometric sensors use an artificial radiation source (e.g. Cs-137; X-ray fluorescence spectrometers, neutron probes) for direct element detection while passive sensors (e.g. gamma-ray detectors) evaluate the natural radioactive radiation of the soil by means of different isotopes.

g) Others: Less common sensors such as capillary electrophoresis, gas sensors, nuclear magnetic resonance spectroscopy, biosensors.

Basically, more than one soil attribute can affect measurements of a distinct proximal soil sensor. This is called the matrix effect. The strength of the matrix effect depends on the selectivity of the sensor. There is often a tradeoff between the selectivity of a sensing principle and its performance in terms of speed, cost, simplicity, robustness etc. Many of the sensors suitable for proximal soil sensing lack selectivity. However, combining data from multiple sensors may address this issue; some sensors can complement each other, which may lead to a wider spectrum of detectable soil properties as well as more accurate and reliable predictions (Adamchuk and Viscarra Rossel, 2010; Javadi et al., 2021; Ji et al., 2019; Munnaf et al., 2020; Xu et al., 2019a; Zhang and Hartemink, 2020).

Considering temporal dynamics of some soil properties (e.g., soil moisture and pH) in the field, the optimal way to collect sensor data that are supposed to be fused, would be conducting the measurements for all of them simultaneously. This requires an integration of different proximal sensing technologies into a single multi-sensor platform. Sensor fusion might help to filter out the matrix effect, makes the measurements more time- and labor-efficient than doing them individually with each single sensor, and finally, reduces field traffic.

In recent years, various sensor combinations have been evaluated for soil sensing (Javadi et al., 2021; Ji et al., 2019; La et al., 2016; Mahmood et al., 2012; Mouazen et al., 2014; Vogel et al., 2022; Xu et al., 2019a; Xu et al., 2019b). However, most of these studies were conducted either in the laboratory or in the field using non-integrated sensor systems.

To the best of our knowledge, three manufacturers commercially offer mobile multi-sensor platforms for soil mapping: Veris Technologies (USA), Shibuya Seiki Co., Ltd. (Japan), and Geophilus GmbH (Germany).

Veris Technologies is offering two integrated systems, MSP and U3, which are based on ECa (using galvanic contact instrument), pH and two-wavelength optical sensing. The main difference between the two Veris platforms lies in their pH sensor modules. MSP uses the Soil pH Manager™, developed based on Adamchuk et al. (1999), for on-the-go pH measurements, whereas U3 uses a pH module for stop-and-go measurements. A complete description of the MSP platform has been presented by Vogel et al. (2022). Inter alia, the Veris MSP has been successfully employed for predicting site-specific lime requirements (Bönecke et al., 2021; Vogel et al., 2022).

The Shibuya platform (named as SAS, the current version is SAS3000; Kodaira and Shibusawa (2020)) includes a Vis-NIR spectrometer as its main sensor. However, calibrations are only available for Japanese soils (Kodaira and Shibusawa, 2013, 2020).

The Geophilus measurement system (Lueck and Ruehlmann, 2013) comprises a multi-depth electrical resistivity sensor and a gamma-ray sensor. The Geophilus system is mainly used for commercial mapping services provided by the company. It has been used successfully for soil texture mapping (Bönecke et al., 2021).

In this study, we present a recently developed, state-of-the-art multi-sensor platform for high-resolution topsoil mapping, the so-called RapidMapper, which includes more and more advanced sensors than those of the aforementioned commercial systems. The main objective of the research presented here is to show how a combination of these – and potentially other – sensors can be achieved by deploying them on a single platform to secure their spatio-temporal alignment. We describe the platform's technical setup and functionalities, and present tests on different soils across Germany. These include analyzing sensor response to different ambient conditions, evaluating measurement consistency over time and comparing data with other platforms and against laboratory measurements.

2. Materials and methods

2.1. The mobile multi-sensor platform

Within the BonaRes project I4S: Intelligence for Soil (https://www.bonares.de/i4s), a multi-sensor platform, called RapidMapper, has been developed for on-the-go topsoil mapping. In the following subsections, we describe the platform and its four proximal soil sensors.

2.1.1. The platform

The platform was designed in-house to serve as a scientific tool, which enables the deployment of several sensor technologies in an easy way. Thus, it offers extensive space for mounting different sensor modules. It has its own power supply and four wheels to make it independent from the type of towing vehicle.

The platform (as shown in Fig. 1) is composed of two main chassis frames, one is fixed (relative to the ground) and the other one is movable (up- and downwards). It has been designed in this manner to toggle all sensors in parallel into travel or work mode. When the platform is in travel mode, the movable frame (indicated in dark blue color in Fig. 1) is in its highest position, and when it is in work mode, the frame is in its lowest position. It is moved by four linear actuators installed in the four corners of the platform (see the top view in Fig. 1B); and it is controlled either manually by push buttons on the control panel or by remote control.

Fig. 1 shows CAD models of the RapidMapper platform for both, travel and work mode. Its weight is about 800 kg (water tank empty). The overall dimensions as well as the main parts of the platform are specified in the figure. Parts such as: drawbar, which connects the platform to a towing vehicle, four linear actuators, which lift and lower the movable frame, wheels, the foldable frame which holds the gamma-ray sensor, two linear actuators, which fold and unfold the foldable frame, power generator, air compressor and accumulator, water tank, and differential global navigation satellite system (DGNSS) receiver, among others, are installed on the fixed frame. In contrast, operating parts including the rolling electrodes of the ECa system, the furrow opening "shoe" of the optical sensor, and the pH sensor module, which have to be in direct contact with the soil during measurements, are mounted to the movable frame.

The platform can be attached to and pulled by a tractor or an off-road vehicle via the drawbar (Figs. 1 and 2). To transport the platform to the field, we utilize a specialized trailer (Supplementary Fig. 1). For loading the platform, the rear of the trailer is hydraulically lowered, converting its rear door into a ramp (as shown in Supplementary Fig. 1). The platform is then carefully maneuvered into position at the rear of the tilted trailer, and a robust winch is employed to gradually and smoothly

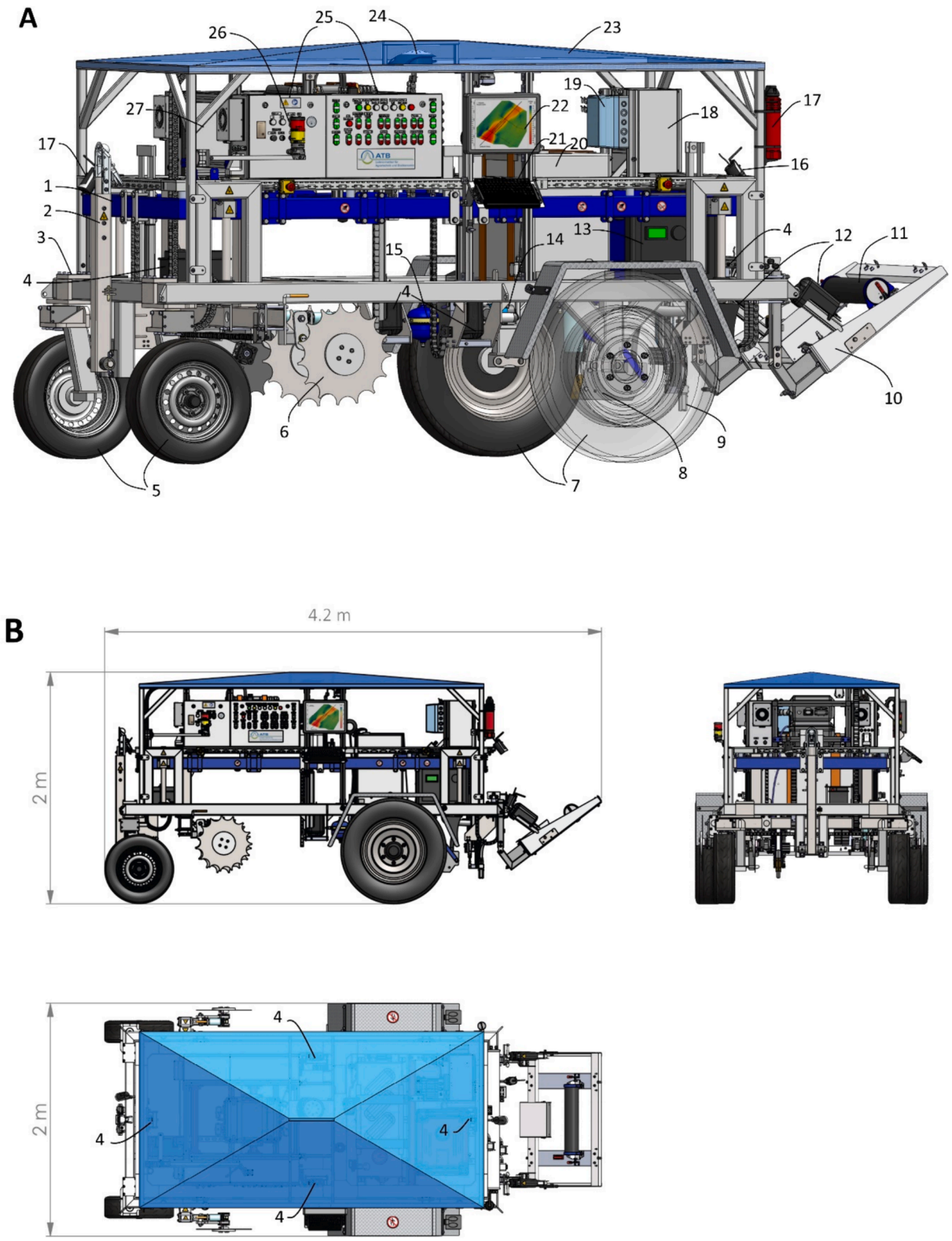

Fig. 1. CAD models of the RapidMapper. **A:** the platform in travel mode, **B:** three-view orthographic projection of the travel mode, **C:** the platform in work mode, and **D:** three-view orthographic projection of the work mode; 1- Movable frame (up- and downward) – outlined by blue color; 2- Drawbar for connecting the platform to a vehicle (foldable); 3- Fixed frame; 4- Linear actuators for lifting and lowering the movable frame; 5- Front wheels; 6- Rolling electrodes of the EC system; 7- Rear wheels; 8- Furrow opening "shoe" for the optical sensor; 9- pH sensor; 10- Foldable frame (for installing the gamma-ray sensor); 11- Gamma-ray sensor; 12- Linear actuators for extending and retracting the foldable frame; 13- Power generator; 14- Air compressor; 15- Air accumulator; 16- Camera; 17- Fire extinguisher; 18- Box of the optical sensor module; 19- pH sensor module; 20- Water tank; 21- Keyboard; 22– Monitor; 23– Roof; 24- DGNSS receiver; 25- Control panel; 26- LED warning lights; 27- Box of the computer. (For interpretation of the references to color in this figure legend, the reader is referred to the web version of this article.)

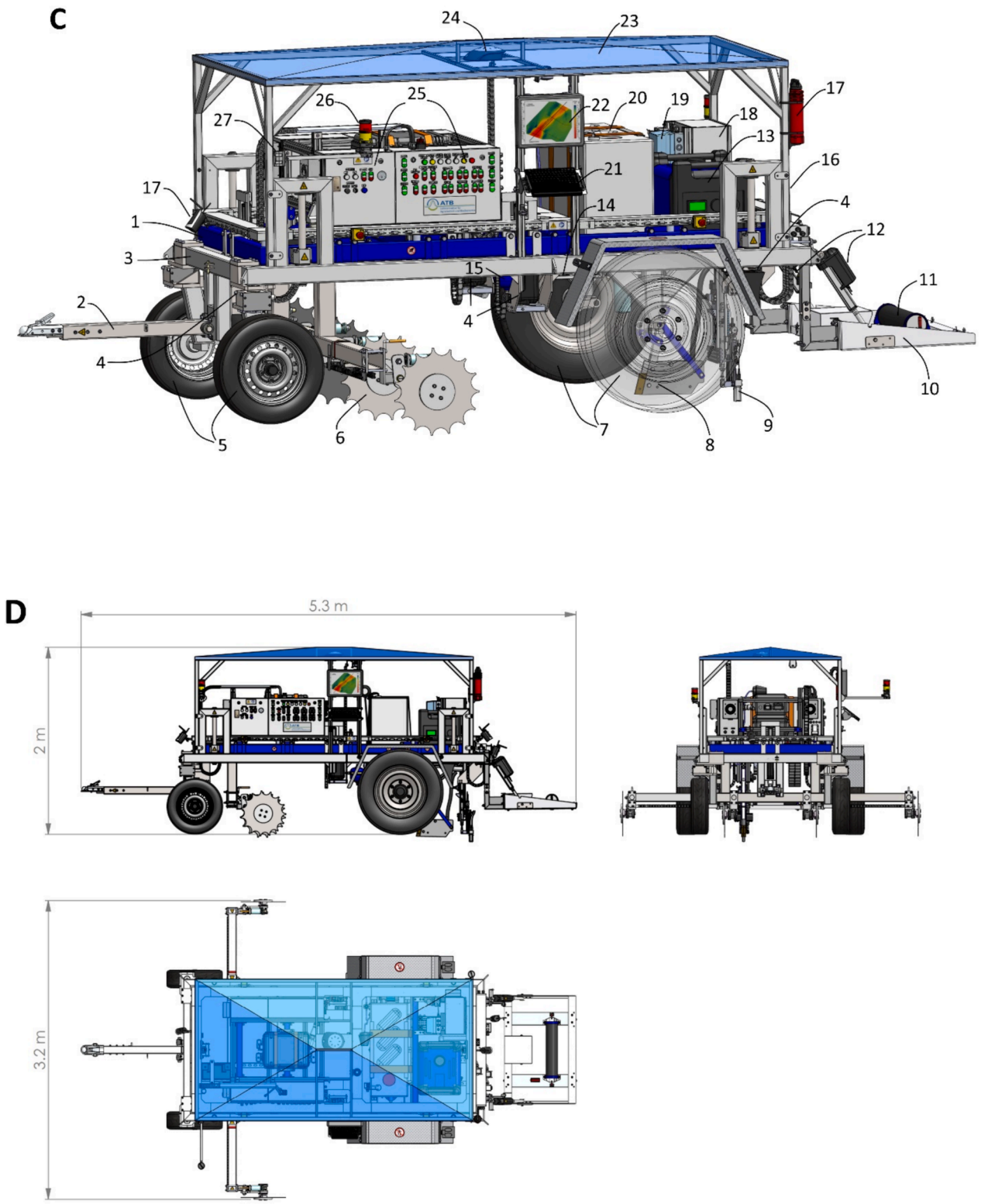

Fig. 1. (*continued*).

pull it upwards until it rests securely on the trailer bed. This method eliminates the need for an external ramp and ensures a smooth loading process. Once the platform is properly positioned on the trailer bed, a series of ratchet straps are used to secure it to the trailer.

2.1.2. Geoelectric sensor

The soil apparent electrical resistivity (ERa) / conductivity (ECa) measuring system of the RapidMapper is based on the galvanic contact resistivity technique. The instrument is from the Geophilus GmbH, Caputh, Germany. ECa electrodes are arranged in a Wenner configuration (Allred et al., 2008), including four rolling electrodes (discs) placed in line and spaced equidistant from each other ($a = 1$ m). Two outer electrodes (current electrodes) inject an alternating electrical current into the soil (2–200 V AC, max. 1 A, 190 Hz), and the two inner

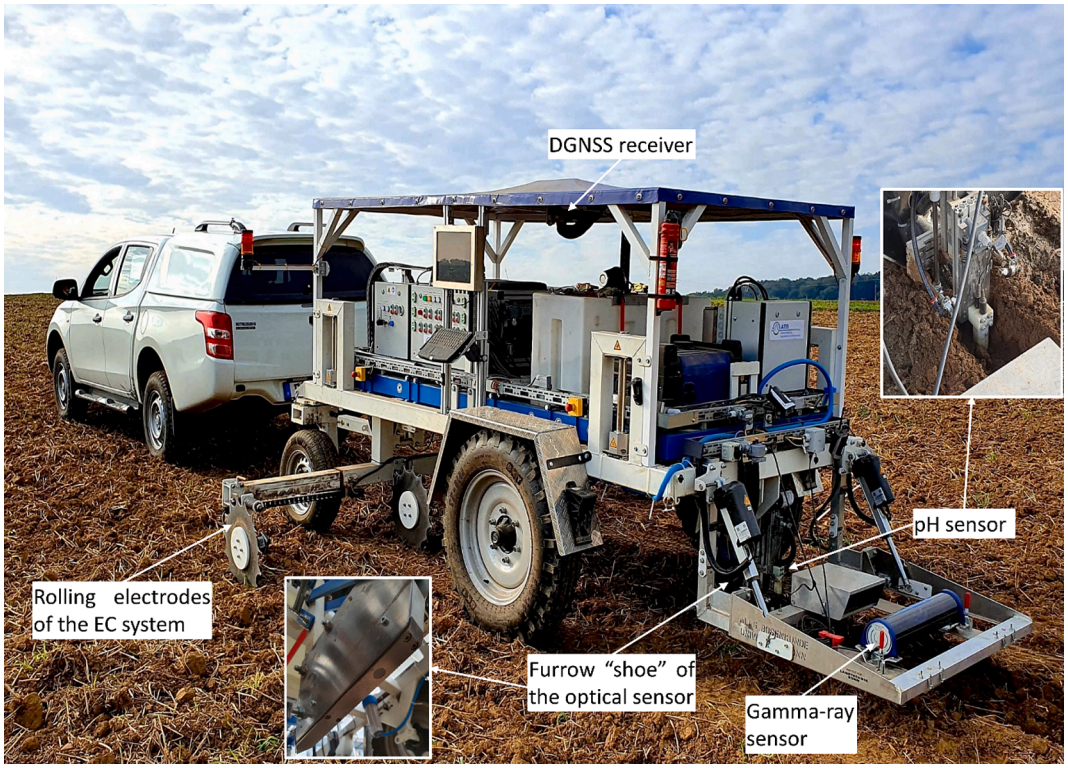

Fig. 2. Image of the RapidMapper platform in working mode.

electrodes (potential electrodes) measure the resulting potential difference, which is recorded at a frequency of 1 Hz. According to Gebbers et al. (2009) the effective depth of investigation for the Wenner configuration is approximately equal to $a/2$. Thus, the system explores the soil ER_a/ECa at about 0–50 cm.

The ERa/ECa is calculated as (Allred et al., 2008):

$$ER_a = \frac{\Delta V}{I} 2\pi a \quad (1)$$

$$EC_a = \frac{1000}{ER_a} \quad (2)$$

where *ERa*, *ECa*, ΔV, *I*, and *a* are apparent electrical resistivity (Ω·m), apparent electrical conductivity (mS/m), potential difference (V), current (A), and inter-electrode spacing (m), respectively.

The measurements are conducted when the platform is in work mode and the rolling electrodes are moved into the soil. The discs are installed on telescopic profiles, so that the two outers can be extended (for work mode, Fig. 1D) or retracted (for travel mode, Fig. 1B).

2.1.3. Gamma-ray sensor

A passive gamma-ray spectrometer (model MS-2000-CsI-MTS, Medusa Radiometrics BV, Groningen, Netherlands) was integrated via a foldable frame that is (i) open towards the soil surface and (ii) is mounted in distance to the platform in order to avoid any attenuation of gamma-rays by the platform. The sensor is composed of a CsI (Caesium Iodide) scintillator crystal of 90 × 310 mm and a 2048-channel MCA (multichannel analyzer). Besides the total gamma-ray emission (total counts, TC), the system can detect the naturally occurring radionuclides, Potassium-40 (^{40}K), Uranium-238 (^{238}U) and Thorium-232 (^{232}Th), as well as the human-made radionuclide, Caesium-137 (^{137}Cs).

The spectrometer covers an energy spectrum of 0 to 3000 keV, however, only the range of 300 to 2900 keV is taken into account for the analysis. In work mode, the gamma-ray detector (Figs. 1 and 2) has a distance of 0.3 m from the soil surface. The data are recorded at a frequency of 1 Hz.

2.1.4. Optical sensor

To measure soil visible and near-infrared (Vis-NIR) diffuse reflectance in the field, a furrow opening 'shoe', similar to that of the Veris OpticMapper (described by Vogel et al. (2022)), was attached to the RapidMapper (Figs. 1 and 2). The shoe was pulled through the soil while the platform moves, allowing the measurement of subsurface soil reflectance at a depth of 10 − 15 cm. As shown in Fig. 2, there is a sapphire window on the underside of the shoe, through which the soil is illuminated and the reflected light is detected.

Currently, a NIR spectrometer (model C11118GA, Hamamatsu Photonics K. K., Shizuoka Pref., Japan), which covers the nominal range of 860 − 2550 nm with an average spectral resolution of 15 nm, is used on the platform. Like the ERa/ECa and the gamma-ray sensor, the optical sensor is recording data at a frequency of 1 Hz. To maintain the accuracy and consistency of NIR measurements, a diffuse reflectance calibration with a reflection reference must be carried out every 30 min.

2.1.5. pH sensor

The current pH module installed on the RapidMapper is used in a stop-and-go manner allowing pH measurements at different spatial resolutions. A mechanism was built (shown in Fig. 2), which allows the up and down movement of two ion-selective antimony pH electrodes by pneumatically operated actuators.

Antimony pH electrodes are particularly suitable for applications under harsh conditions like soil (Vonau et al., 2020) and thus, they are used on the platform. The electrodes are installed right after the NIR shoe, so that the pH measurements are made in the furrow opened by the shoe and in the same depth as the NIR data are collected. After each measurement, the electrodes are cleaned with tap water from a 400 L tank by two spray nozzles. The antimony electrodes are calibrated using standard pH buffer solutions of pH 4.0 and 7.0.

2.1.6. DGNSS receiver

A differential global navigation satellite system (DGNSS) receiver (model AgGPS 162, Trimble Inc., Westminster, Colorado, US) is integrated to the platform to record geographical coordinates and elevation. The receiver provides a pass-to-pass accuracy of around 20 − 30 cm. The DGNSS data are recorded at a rate of 1 Hz. Position data is broadcasted to the sensor modules via a serial port splitter in order to ensure that each sensor receives an identical data stream.

2.1.7. Sensor data acquisition software

Software for instrument control and conducting measurements was implemented under MS Windows 7. For some sensors (NIR and pH), dynamic link libraries (DLLs) were available and we used them to develop C# programs. However, for the other sensors (geoelectric and gamma-ray), we were forced to use software from the sensor provider. Therefore, for each sensor module, there is a separate software, which runs independently.

The sensor modules' software incorporates several key features, including a) controlling sensor operation remotely, enabling fine-tuning sensor parameters b) synchronized sensor and GNSS data logging, c) each sensor's software receives GNSS data from its dedicated serial port – the GNSS data encompasses coordinated universal time (UTC), latitude, longitude, and altitude, among other relevant parameters, d) real-time data visualization for field operators to gain immediate insights into sensor data quality, e) a calibration management section, if required, is integrated into the software, and f) real-time georeferenced sensor data storing on the local hard drive – separate file for each sensor module in a standardized ASCII format (e.g.,.csv or.txt). Our custom software solutions were developed using the C# programming language and the.NET Framework 4.8.

2.2. Sensor data (post-) processing

Data processing flow for each of the sensor modules is given below.

The gamma-ray sensor; The gamma-ray data is processed using the Gamman software (Version 1.42, Medusa Systems, The Netherlands). This process involves the following steps:

- Data points merging: To enhance the precision of radionuclide concentration estimates, we employ a repeated-fit approach that involves merging multiple spectra prior to data analysis. By combining consecutive spectra, we accumulate a higher total gamma-ray count, which effectively reduces the uncertainties associated with radionuclide quantification. However, this strategy trades off spatial resolution, as combining spectra reduces the granularity of spatial information. Additionally, auxiliary data, such as GNSS position, is also averaged to maintain consistency with the merged spectra
- Smoothing: To enhance the overall smoothness of the gamma-ray data, we may apply a moving or running average filter over data point measurements with a user-defined window size. This technique involves calculating the average of a specified number of data points within a sliding window and assigning this average value to the central data point. The window size determines the degree of smoothing, with larger window sizes producing smoother data.
- Gamma-ray analysis: Gamman utilizes the full spectrum analysis (FSA) technique to determine radionuclide concentrations from gamma-ray spectra. Gamma-ray analysis involves a two-step process: i) spectrum stabilization: Each multi-channel spectrum in the dataset is transformed to ensure that all peaks appear at their corresponding energy positions, ii) radionuclide quantification: Each stabilized spectrum is deconvolved to determine the concentrations of various radionuclides, including ^{40}K, ^{238}U, ^{232}Th, and ^{137}Cs in Bq/kg or ppm. For spectrum stabilization, Gamman automatically applies gain stabilization to the imported spectra using the reference spectra provided in the calibration file. Beyond radionuclide concentrations, the gamma-ray analysis outcomes include total counts (TC) or count rate, standard deviations for the radionuclide concentrations, and the chi-squared (χ^2), which is a measure of the goodness of fit in the deconvolution.

The optical sensor; once collected, NIR spectra undergo a series of processing steps:

- Calculation of reflectance: Reflectance is a measure of how much light is reflected by a surface. A perfectly reflecting surface would have a reflectance of 1, while a perfectly absorbing surface would have a reflectance of 0. Most real-world surfaces have reflectances between 0 and 1. The reflected light of soil is converted to reflectance using known reflection properties of a certified reflection standard (Spectralon) and through the following equation:

$$\rho = \frac{\mathrm{R\text{-}R_d}}{\mathrm{R_s\text{-}R_d}} \times \mathrm{Cf} \quad (3)$$

where ρ, R, R_d, R_s, and Cf are reflectance, soil reflection, dark reflection, reflection of the standard reference, and reference correction factor (for each wavelength).

- Filtering out noisy spectra: We eliminate spectra that show atypical characteristics or deviate significantly from the expected pattern of a typical soil NIR spectrum. To automate the process of spectra filtering, we developed an algorithm in MATLAB software (The MathWorks Inc., Natick, MA, USA) that effectively eliminates noisy spectra.
- Picking the median spectrum from each second of measurements: Depending on the integration time of the spectrometer and driving speed of the platform, a few spectra per second would be recorded. To ensure coincidence between the NIR measurements and the data from the other sensors and the GNSS, we select only the median spectrum from each individual second of measurements.
- Edge trimming: NIR spectrometers are generally less sensitive at the edges of their operating range. This means that there is less signal to noise at these wavelengths, which can lead to noisier data. This is particularly evident in field measurements acquired using the spectrometer integrated into the RapidMapper. Therefore, we eliminate the edges of spectra.
- Spectral pre-processing: Under the harsh measurement conditions in the field, various factors such as mechanical vibrations, sudden variation in topography etc. can distort spectra, introducing noise across the entire wavelength range (Mouazen et al., 2009). Therefore, the spectra need to be pre-processed by approaches such as Savitzky–Golay smoothing (Savitzky and Golay, 1964), in order to eliminate the noises.

The geoelectric sensor; we employ equations (1) and (2) to transform the raw measurements obtained from the geoelectric system into apparent electrical conductivity values.

The pH sensor; to ensure data reliability, we implement a quality control procedure for pH measurements acquired using two antimony electrodes. At each measurement point, we compare the pH values obtained from both electrodes. If the values are within a predefined tolerance range, we average them to derive a more accurate pH determination. However, if the difference between the electrode readings exceeds the tolerance limit, we discard the measurement as potentially erroneous.

Post-mapping; we visualize the data of all sensors using QGIS software (QGIS.org, 2023) to graphically examine the distribution of the values and identify any potential errors or inconsistencies in the measurements.

2.3. Soil mapping with the platform

2.3.1. Field campaign

The general functionality of the RapidMapper was evaluated in different soilscapes across Germany (Fig. 3). Table 1 summarizes key information about the test sites, including their size, reference soil groups and locations, as well as the dates of mapping. For the detailed data quality assessment, we focused on the Marquardt and the Booßen site. The Marquardt site is an eight-plot sensor test site that has been artificially constructed within the "Fieldlab for Digital Agriculture", an experimental station of the Leibniz Institute for Agricultural Engineering and Bioeconomy (ATB), situated in Brandenburg (Germany). Each plot encompasses an area of 12 × 12 m and a depth of 30 cm. Four different soils, including sandy-low in SOM, sandy-rich in SOM, clayey-no SOM, and silty-no SOM, were introduced in two replications. The Booßen field test site is an agricultural field under conventional management in the east of Brandenburg exhibiting high spatial variability in soil properties. From this site, a high amount of sensor data exist that were collected over three consecutive years (Schmidinger et al., 2024; Vogel et al., 2022).

The RapidMapper platform was pulled over the fields at an average speed of 2.5 km/h and along parallel transects.

2.3.2. Sensor data

2.3.2.1. The RapidMapper's data. From the geoelectric sensor, soil apparent electrical conductivity (ECa, mS/m) values were directly obtained. The gamma-ray raw measurements were processed using the GAMMAN software and concentrations of the radionuclides (in Bq/kg): Potassium-40 (^{40}K), Uranium-238 (^{238}U), Thorium-232 (^{232}Th) and Caesium-137 (^{137}Cs) were estimated based on respective calibration of the sensor by the manufacturer. Since the NIR spectra were noisy at the edges of the wavelength range, only the range of 900–2450 nm (with 1 nm intervals) was used. From the pH sensor, the mean values of the pH measurements of the two ion-selective antimony electrodes were calculated.

2.3.2.2. Laboratory-based data. In September 2020, soil samples were collected across the Booßen field using a systematic sampling design (Fig. 3). Samples were taken from a depth of 0–30 cm along three parallel transects spaced 12 m apart. A total of 159 samples were collected at 15-meter intervals along transect. After being oven-dried at 75 °C and sieved to a particle diameter of less than 2 mm, the soil samples were scanned by the spectrometer described in section 2.1.4 for laboratory-based NIR analysis. Inside a light-controlled chamber, four halogen lamps positioned at a 45-degree angle provided uniform illumination for the samples. The final spectra had a range of 900 to 2450 nm with a resolution of 1 nm.

Table 1
Detailed information about the fields mapped by RapidMapper.

Study site	Parent material *	Reference soil groups **	Area (ha)	Location coordinates	Mapping date(s)
Marquardt	Boulder clay covered by glacial sands	Cambisol, Luvisol	0.1	52°27′25.4″N, 12°57′55.9″E	August 2020
Booßen	End moraine glacial till	Luvisol, (Calcaric) Regosol	40	52°22′16.8″N, 14°28′21.1″E	April 2020 – August 2021 – August 2022
Bölingen	Loess, Loess loam	Luvisol, Stagnosol	2.8	50°34′1″N, 7°5′5″E	September 2020
Görzig	Loess	(Gleyic) Chernozem	65	51°39′50″N, 11°59′48″E	August 2021
Suderburg	Boulder clay covered by glacial sands	(Albic) (Stagnic) Cambisol, (Stagnic) Luvisol	15	52°53′46.9″N, 10°26′44.0″E	February 2021
Hermersdorf	End moraine glacial till	Luvisol, (Calcaric) Regosol	1.6	52°34′03.8″N, 14°10′59.8″E	September 2022

* The parent material was obtained from (BGR) (2013).
** The reference soil groups were retrieved form Group (2015).

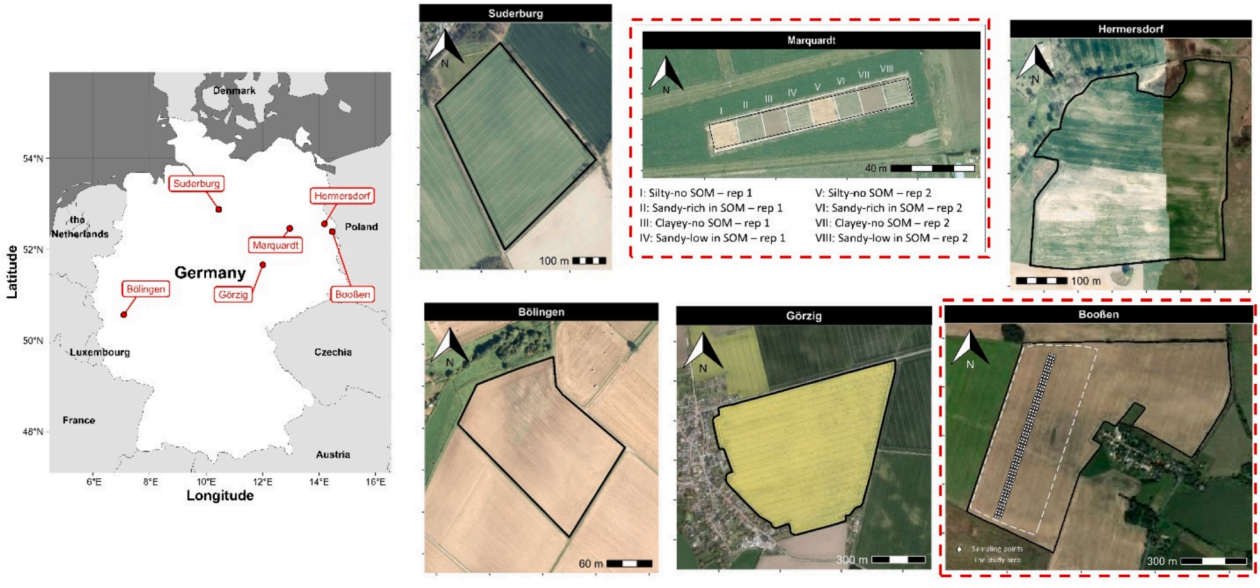

Fig. 3. Overview of the agricultural fields mapped by the RapidMapper platform in Germany. The geographical locations are shown on the left map. Black lines delineate the boundaries of each field. The red dashed frames highlight the two focus fields of this paper: The sensor test site in Marquardt with four different soils and the Booßen field including the study area and the locations of reference sampling points. (For interpretation of the references to color in this figure legend, the reader is referred to the web version of this article.)

2.3.2.3. Data from other sensor platforms. In August 2021, while conducting the RapidMapper survey at the Booßen field, we also mapped the field using two separate platforms concurrently: The Veris MSP (described in Vogel et al. (2022)) and the Geophilus platform (Lueck and Ruehlmann, 2013). The Veris MSP platform utilizes a galvanic coupled resistivity instrument with six parallel rolling coulter electrodes. This instrument measures soil apparent electrical conductivity at two depths: Shallow (ECsh) with an effective exploration depth of 0–12 cm and deep (ECdp) with an effective exploration depth of 0–37 cm (Gebbers et al., 2009; Vogel et al., 2022). The Geophilus platform features seven pairs of rolling electrodes that measure soil electrical conductivity at various effective depths down to 1.5 m. It also includes a gamma-ray sensor to detect the total gamma-ray counts emitted by the soil per second (Bönecke et al., 2021; Lueck and Ruehlmann, 2013). In this study, we focused only on the ECa data collected from the shallowest depth layer (0–25 cm) by the Geophilus system.

In 2017, the Booßen field was mapped for EC and gamma-ray radiation using the Geophilus platform (Bönecke et al., 2021). Additionally, the Veris MSP captured EC, near-infrared (NIR), and pH measurements in 2017, followed by another campaign of EC and pH measurements in 2018 (Vogel et al., 2022). The field NIR data ranged from 1100 to 2100 nm, with an average resolution of about 5 nm.

In November 2020, we additionally compared RapidMapper's gamma-ray sensor with a RSX-1 gamma-ray spectrometer (Radiation Solutions Inc., Canada) at the Booßen field. The RSX-1 has been demonstrably effective in a number of previous studies (Heggemann et al., 2017; Pätzold et al., 2020). It consisted of two 4.2 L thallium activated sodium iodide (NaI(Tl)) crystals mounted on a tractor's three-point hitch using a steel frame. This instrument captured gamma-ray spectra at a rate of 1 Hz with 1024 channels. For comparison, we selected 36 representative points from the 159 sampling locations, ensuring coverage across the entire range of clay content and gamma-ray emission. At each of these points, both instruments performed stationary measurements for 60 s. This way, measurements were co-located and less noisy. For a more detailed description of the methodology, please refer to Pätzold et al. (2020).

2.3.3. RapidMapper's functionality and data quality assessment

The functionality of the RapidMapper platform and the quality of its collected data were evaluated through:

i. General functionality assessment: Assessing the functionality of the platform for consistent mapping of various fields across Germany.
ii. Sensitivity assessment: Assessing the response of the sensors to different soils at the Marquardt sensor test site.
iii. Temporal consistency assessment: Measurements from the Booßen field taken in April 2020, August 2021, and August 2022 were evaluated for consistency over time.
iv. Similar sensors' comparison: RapidMapper's ECa, gamma-ray and NIR sensors were compared with other devices using the same measurement principle. ECa measurements from RapidMapper were compared to those from Veris MSP and Geophilus devices in the Booßen field (August 2021). Readings from RapidMapper's gamma-ray sensor were compared with those of a RSX-1 gamma-ray spectrometer (Radiation Solutions Inc., Canada). NIR data collected by the RapidMapper in the Booßen field was compared to data from the Veris MSP.
v. *In-situ* vs. laboratory measurement's comparison: NIR data collected in the field using RapidMapper was compared to laboratory analysis results from the Booßen field using correlation analysis.

2.3.4. Data analysis

For the general functionality assessment: Visualization of the sensors' data for all the fields and campaigns was done.

For the sensitivity assessment: We investigated differences in RapidMapper sensor readings across the plots of four different soil types at the Marquardt sensor test site using analysis of variance (ANOVA). The parameters analyzed included NIR total reflectance (calculated as the sum of reflectance values across the NIR spectra for each measurement point), gamma total counts, ECa, and pH value. Tukey's Honest Significant Difference (HSD) test was used as a multiple comparison procedure to identify specific plots with significantly different readings. It is important to note that pH data was not analyzed with ANOVA because only one measurement per plot was available. The NIR spectra of the different soil types were also visualized.

For the temporal consistency assessment: To ensure consistent spatial comparisons across all measurement campaigns in the Booßen field, we restricted our analysis to the common area (intersection) where data was collected by all campaigns. Raster maps were generated for gamma-ray total counts and ECa data. To standardize the spatial resolution of the raster graphing, sensor measurement points, which were not co-located, were interpolated to a regular grid of 6,818 points delimited by the intersection area. Additionally, we calculated Spearman's rank correlation coefficient (ρ) to analyze the correlation between sensor variables (in the case of NIR data: total reflectance). The NIR spectra of the intersection area were also visualized.

For the similar sensors' comparison: We calculated Spearman's rank correlation coefficient (ρ) to assess the correlation between different sensors' readings, and created raster maps for the ECa data from the different devices. Since the Geophilus platform measures apparent electrical resistivity, we converted its data to ECa for easier comparison. To simplify data interpretation and visualization, we scaled all ECa measurements from RapidMapper, Veris MSP, and Geophilus to have a zero mean and unit standard deviation, despite minor variations in their original ranges. Since original measurement points from the different systems were not co-located, we aligned the data spatially by creating a regular grid of 7,972 points within the 2021 RapidMapper survey area for each sensor's ECa data.

For the *in-situ* vs. laboratory measurement's comparison: We analyzed the correlation between lab and field NIR total reflectance data using Spearman's rank correlation coefficient (ρ). The NIR data underwent pre-processing. This included standardizing the reflectance data using standard normal variate (SNV) transformation and interpolating the RapidMapper and Veris MSP data for spatial alignment with the reference sampling locations (the 159 sampling points) using ordinary block kriging from the "gstat" library in R (Pebesma, 2004) with a block size of 10×10 m^2. To expedite the interpolation process, we considered only the 500 reflectance measurement points that were spatially closest to each target point. A variogram was automatically fitted for each sensor variable using the 'automap' library of R (Hiemstra et al., 2009). This routine iterates over the variogram models (spherical, exponential, Gaussian, etc.) and selects the model that has the smallest residual sum of squares with the empirical variogram. The median NIR reflectance spectra (after SNV transformation) of the lab and field measurements were also visualized.

Data management and visualization were done in R (Team, 2019) using the 'tidyverse' packages (Wickham et al., 2019). The satellite images presented in this paper were acquired from Esri World Imagery Basemap using the 'basemaps' library of R (Schwalb-Willmann, 2024). All the data analyses were done on a single machine with the following specifications: Intel Core i7-10850H, 2.70 GHz, 6 cores, 12 logical processors; 16 GB RAM; Windows 10.

3. Results and discussion

3.1. Assessing the general functionality of the RapidMapper

The RapidMapper's ability and consistency for soil mapping was successfully tested on 6 test sites across Germany from 2020 to 2022. Supplementary Fig. 2 visualizes sensor data collected for each field.

Additionally, Supplementary Fig. 3 presents the NIR reflectance spectra for the fields, which follow the typical soil spectrum format. Comparison of the spectra between the fields reveals significant variations, linked to differences in soil properties. This is exemplified by the spectra of the Marquardt field (Fig. 4), where four different soils with different properties led to distinct variations in the spectra.

Initial tests of the RapidMapper in the fields showed promising results. While the system allows for the simultaneous operation of multiple soil sensors, its complexity can lead to errors. Notably, using Microsoft Windows as the operating system appears to cause issues with the timing of commands being sent and data being received. Our field tests revealed that for the RapidMapper platform to function optimally, some level of field preparation is necessary. In particular, it is crucial to remove or chop plant residues in front of the NIR shoe for optimal performance. Our experience suggests that the geoelectric sensor's readings are significantly impacted by very dry soil conditions. This is an important factor to consider when scheduling field campaigns.

3.2. Sensitivity assessment of the RapidMapper's sensors

Fig. 4 presents visualizations from sensor data acquired by RapidMapper in the Marquardt sensor test site. To summarize the sensor readings, we calculated mean values and standard errors for each sensor data. Additionally, for the NIR data, we calculated the mean values of total reflectance alongside visualizing the spectra. The data reveals a consistent pattern: Comparisons of both the mean sensor values (Fig. 4A) and the NIR spectra (Fig. 4B) show a clear reflection of the different soil properties of the four soil types in the sensor readings. This is true for all measurements except for pH, where the values across the four soils are relatively similar. However, this rather small pH variability of the plots was also reflected by standard lab-based pH measurements. For plots with repeated soil types, high similarity in sensor values and NIR spectra is evident.

Interestingly, both the mean total reflectance and the NIR spectra show a similar pattern: Plots with sandy-low in SOM soil and sandy-rich in SOM soil have nearly identical spectra shapes, with slightly higher reflectance in the sandy-low in SOM plots. This finding exemplifies the ability of NIR measurements to reflect soil texture and soil organic carbon, as a different SOM content is the primary difference between these two plots, which is visible in a decrease of the NIR reflectance (Nocita et al., 2015). In addition, as expected (Stenberg et al., 2010), clayey plots showed the lowest reflectance (highest absorbance).

Soil texture and gamma-ray emissions are linked, with higher clay content in most cases leading to increased gamma-ray total counts due to the presence of naturally occurring radioactive elements like potassium (^{40}K) and thorium (^{232}Th) within clay minerals (Gebbers, 2018; Heggemann et al., 2017). This typical relationship is evident in the RapidMapper gamma-ray measurements from the sensor test site, showing highest gamma total counts for the clayey soils and lowest total counts for the sandy soils (Fig. 4A). However, negative correlation between clay content and gamma-ray emission has also been reported (Heggemann et al., 2017; Pätzold et al., 2020).

Soil texture significantly impacts apparent electrical conductivity (ECa) (Allred et al., 2008; Gebbers, 2018). The RapidMapper's ECa system reflects this, with sandy soils exhibiting the lowest conductivity, while clayey and silty soils show higher values (Fig. 4A). Nevertheless, the ECa values measured in this August 2020 campaign were generally low, likely due to the typically dry conditions associated with this season. Soil moisture content influences electrical conductivity, as higher moisture enhances the mobility and abundance of ions (dissolved salts), consequently raising the conductivity and vice versa (Hardie, 2020).

Minimal differences in pH measurements between plots with varying textures were observed, except for slightly lower pH values in clayey plots. Clayey soils have a large surface area due to tiny size of their particles. This allows them to hold onto charged particles (cations) more tightly, including positively charged hydrogen (H+) ions, which contribute to soil acidity. Consequently, soils with higher clay content tend to be more acidic (lower pH).

3.3. Temporal consistency assessment of RapidMapper's measurements

We investigated the temporal consistency of RapidMapper's measurements by mapping the Booßen field in three consecutive years: 2020, 2021, and 2022. Unfortunately, no pH data was collected in 2021 (Supplementary Fig. 2). As the pH value is a dynamic soil property, we excluded it from the temporal consistency evaluation. Instead, we focused on ECa, gamma-ray, and NIR data, which should reflect more stable soil properties like texture and SOM. Fig. 5 illustrates the correlation between the sensor data collected across the three years. Additionally, Fig. 6 presents the raster maps of gamma-ray and ECa data, and the NIR reflectance spectra acquired by RapidMapper for the three years.

For assessing the temporal consistency of measurements, in this section we compare correlations of the same variables across the three years. When comparing 2020 and 2021 campaigns, there were strong correlations for gamma-ray total counts (TC), ^{40}K, ^{232}Th, and ECa, good correlations for ^{238}U, and weak correlation for ^{137}Cs and NIR total reflectance. In the case of 2021 and 2022 campaigns, strong correlations for TC, ^{40}K, ^{232}Th, ^{238}U, and ECa, good correlation for ^{137}Cs, and weak correlations for NIR total reflectance were observed. Finally, comparison between 2020 and 2022 data revealed strong correlations for TC, ^{40}K, ^{232}Th, ^{238}U, and ECa, good correlations for NIR total reflectance, and weak correlation for pH and ^{137}Cs.

As shown in Fig. 6A&B, the raster maps for gamma total count (TC) and ECa exhibited high similarity between the 2020 and 2021 campaigns. In contrast, the 2022 data revealed lower similarity. This difference can likely be attributed to the very dry condition during the 2022 campaign. As compared to gamma-ray and ECa data, temporal consistency of NIR data is weaker due to the higher sensitivity of NIR reflection to various factors like soil moisture content. However, the spectra from all the three campaigns maintained the characteristic shape of a typical soil NIR spectrum (Fig. 6C), indicating overall consistency in data acquisition.

Overall, the findings presented in this section support the temporal consistency of RapidMapper measurements from the Booßen field.

3.4. Similar sensors' comparison

Comparison of raster maps generated from ECa data collected by RapidMapper, Veris MSP, and the Geophilus platform in Booßen (August 2021) demonstrated strong concordance (Fig. 7), suggesting these instruments provide comparable measurements of soil electrical conductivity. Furthermore, strong correlations between ECa data of RapidMapper in 2020, 2021 and 2022 with ECa data from Veris MSP and Geophilus in 2017, 2018, and 2021, confirm this observation (Fig. 5). The consistent agreement across multiple instruments and years underpins the reliability of ECa data collected by RapidMapper.

Measurements from the two gamma-ray spectrometers at the Booßen site showed excellent agreement across the entire range of total counts (Fig. 8). This high level of coincidence demonstrates the effectiveness of RapidMapper's gamma-ray sensor for soil sensing.

3.5. In-situ vs. Laboratory measurement's comparison

This section compares NIR data collected *in-situ* by RapidMapper, Veris MSP, and laboratory analysis for the Booßen field. Compared to lab-based measurements, *in-situ* measurements are generally affected by the field conditions during the sensor measurement campaign such as: (i) different soil moisture contents and temperature (while in-situ NIR measurements were conducted on moist soil in the field, the laboratory analyses were conducted on dried samples), (ii) different measurement modus (in contrast to lab NIR measurements, on-the-go *in-situ* NIR

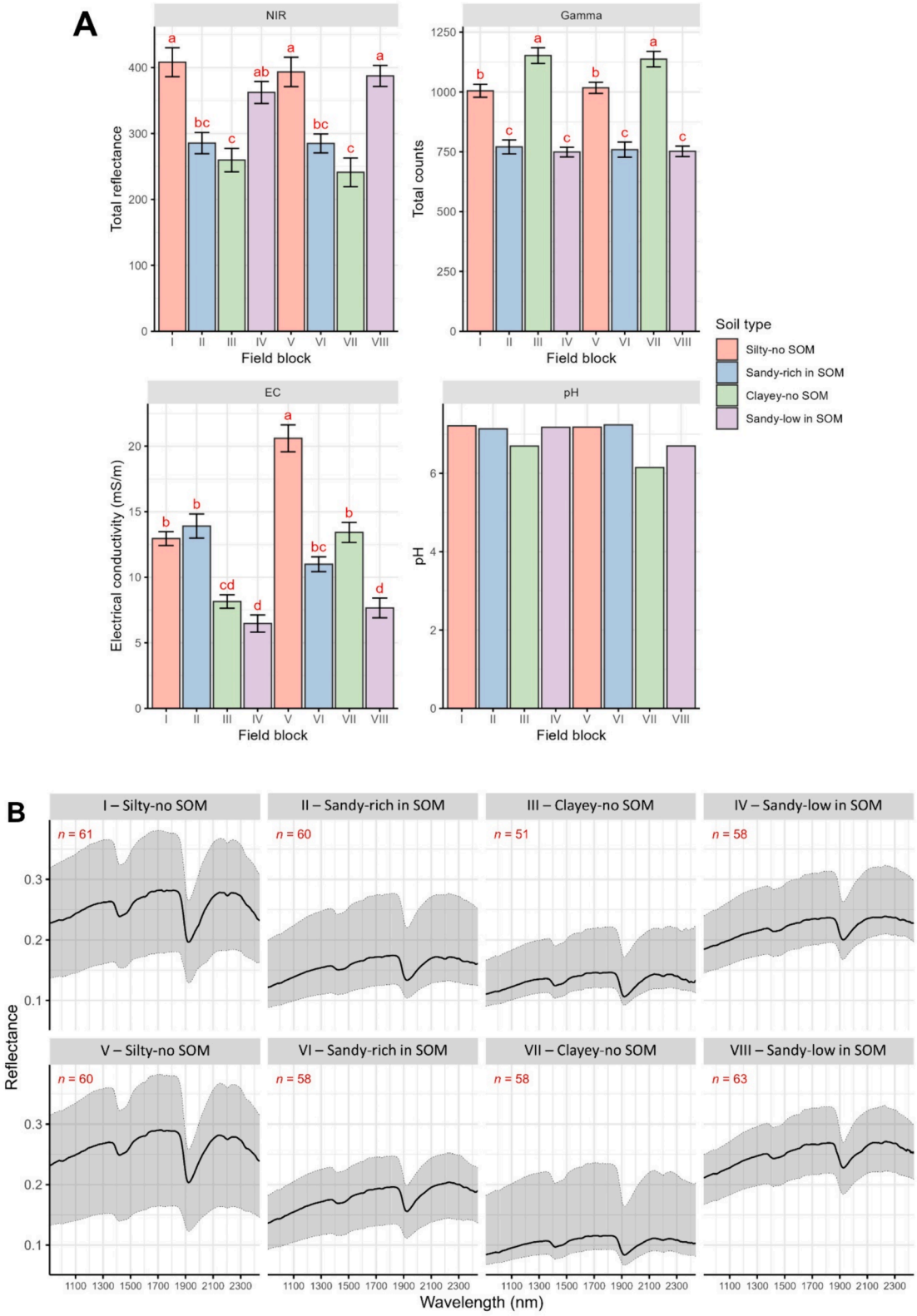

Fig. 4. RapidMapper's sensor measurements from the four different soil types of the sensor test site in Marquardt. **A**: Mean and standard error for sensor readings of RapidMapper within each plot. Means followed by different letters indicate statistically significant differences according to the Tukey test (P-value ≤ 0.05). Note that there was one pH measurement value for each plot; therefore, ANOVA analysis was not conducted for this variable. **B**: NIR reflectance spectra acquired by RapidMapper for each plot. The solid black curve denotes the median value of reflectance at each wavelength. The gray area describes the interquartile interval, with the lower and upper limits corresponding to the first and third quartiles, respectively. Numbers in red indicate the total count of measurement points (*n*). (For interpretation of the references to color in this figure legend, the reader is referred to the web version of this article.)

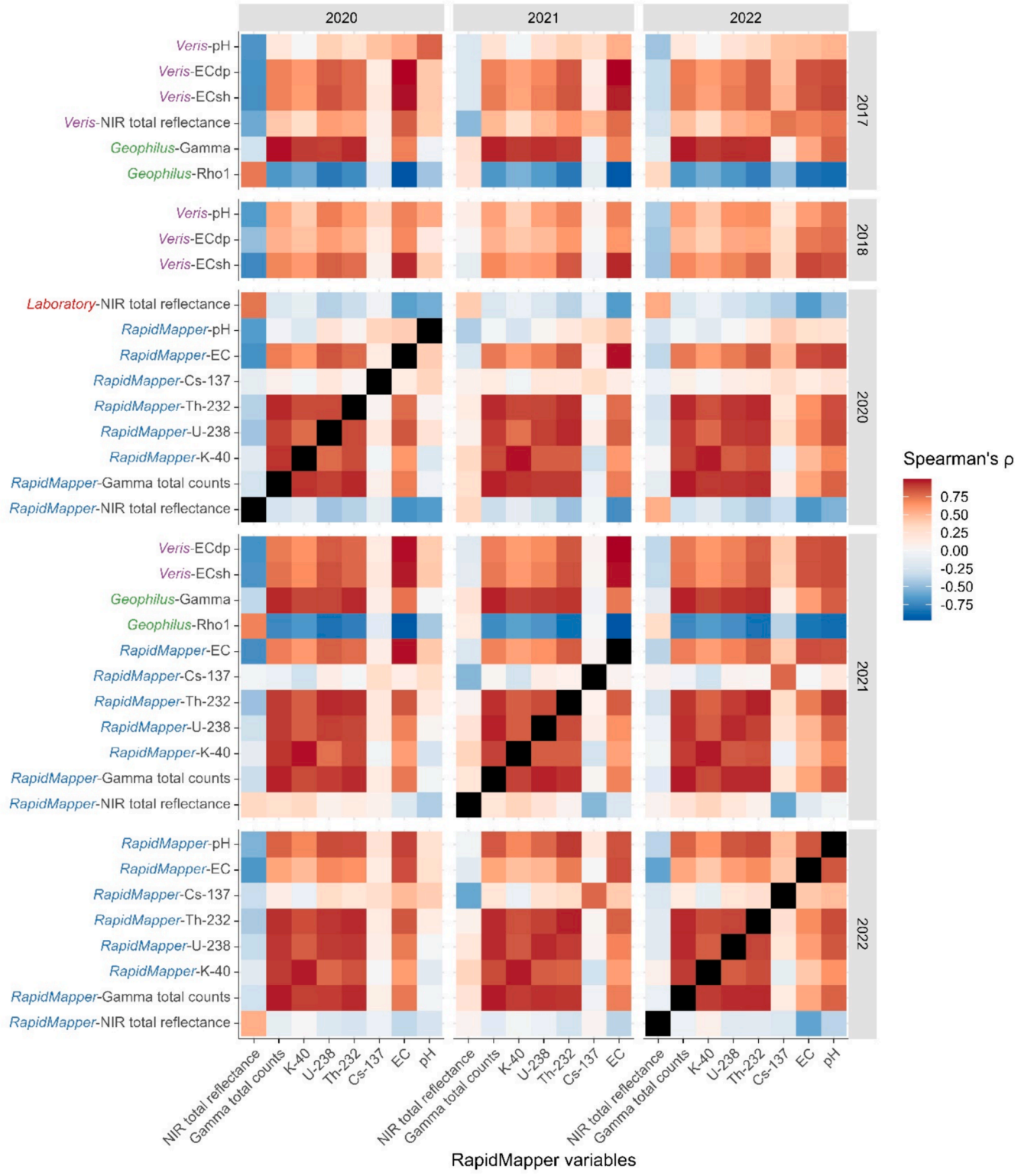

Fig. 5. Correlation matrices for sensor data collected from the Booßen field in three years. RapidMapper sensors are on the x-axis and sensor data from other sensor platforms are on the y-axis. Each cell displays Spearman's correlation coefficient (ρ), ranging from −1 (perfect negative correlation) in deep blue to 1 (perfect positive correlation) in deep red. Black cells represent the correlation of a variable with itself (always perfect, $\rho = 1$). The color intensity reflects the strength of the correlation. We used just 159 sampling locations for this correlation matrix because the lab-based NIR data from these points was the most limited dataset. (For interpretation of the references to color in this figure legend, the reader is referred to the web version of this article.)

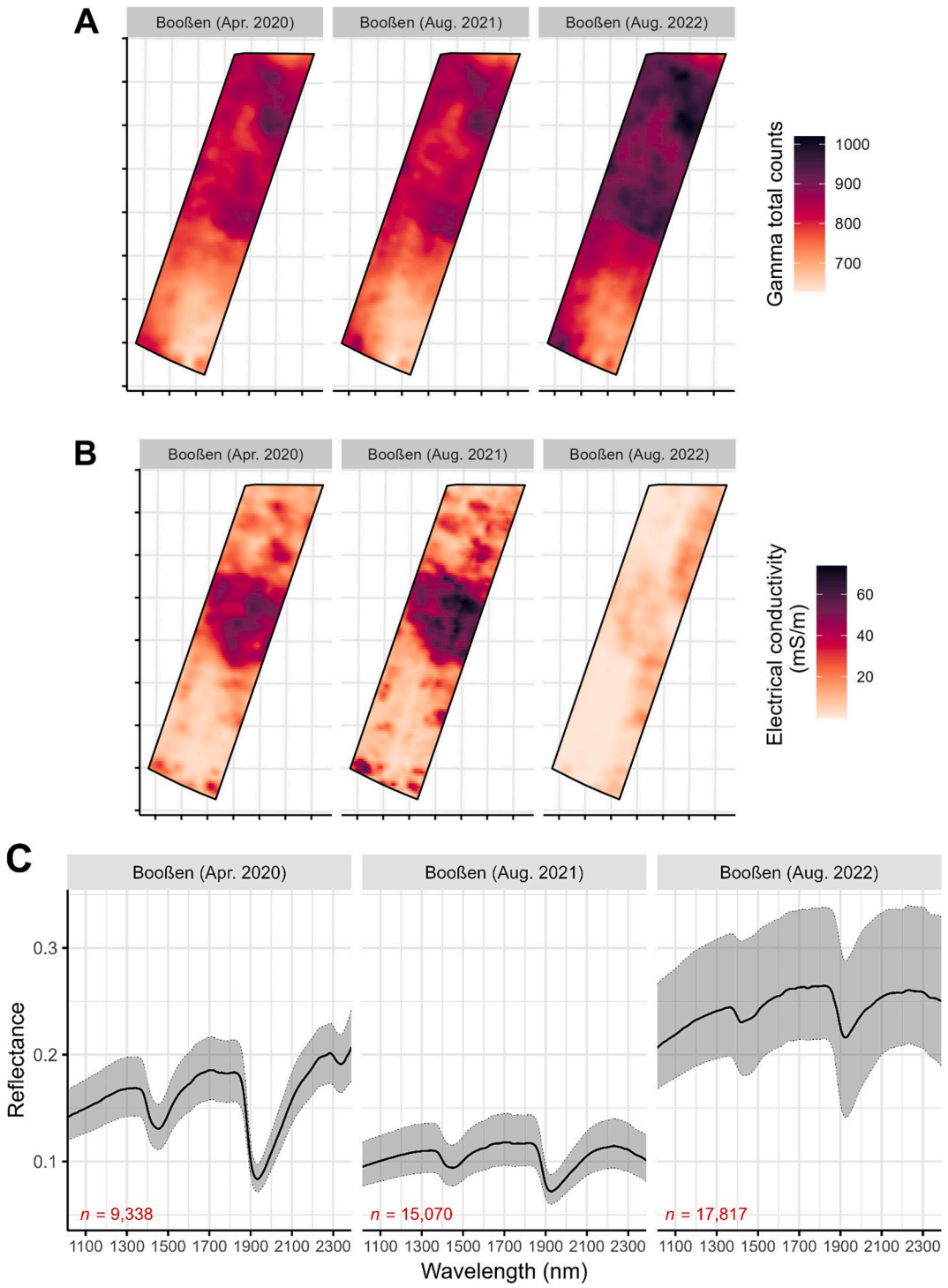

Fig. 6. RapidMapper sensor measurements over three years in the Booßen field. **A:** Raster maps of gamma-ray total counts; **B:** Raster maps of apparent electrical conductivity (ECa); **C:** NIR reflectance spectra acquired by RapidMapper. The solid black curve denotes the median value of reflectance at each wavelength. The gray area describes the interquartile interval, with the lower and upper limits corresponding to the first and third quartiles, respectively. Numbers in red indicate the total count of measurement points (*n*). (For interpretation of the references to color in this figure legend, the reader is referred to the web version of this article.)

measurements are conducted during movement and can be affected by disturbing factors like mechanical vibration (Mouazen et al., 2009)). Despite these limitations, comparing these datasets can provide valuable insights into the quality of RapidMapper data. Section 3.3 demonstrated the challenges of comparing field NIR data from even the same NIR instrument across different years. However, this section explores a comparison between Veris MSP data (2017) and RapidMapper data collected in the Booßen field across multiple years (2020, 2021, and 2022). This comparison, despite the inherent challenges, can offer insights into the agreement of NIR measurements captured by different platforms in the same field.

Fig. 9 displays the median NIR reflectance spectra after SNV standardization for the laboratory and field measurements. Despite generally similar spectral patterns, particularly among field spectra, the laboratory and field spectra differ in the depth of the two valleys around 1400 and 1900 nm. This variation can be attributed to the influence of

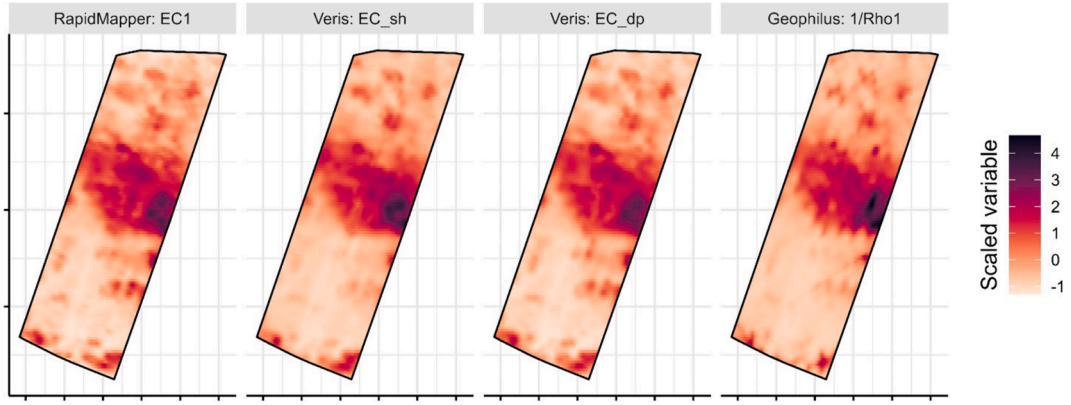

Fig. 7. Comparison between raster maps of soil apparent electrical conductivity (ECa) measurements of the RapidMapper, Veris MSP and Geophilus platforms, collected from the Booßen field in August 2021. Although all sensors directly measure soil ECa, slight differences in their ranges exist. To facilitate data interpretation, each variable was scaled to have a mean of zero and a standard deviation of one.

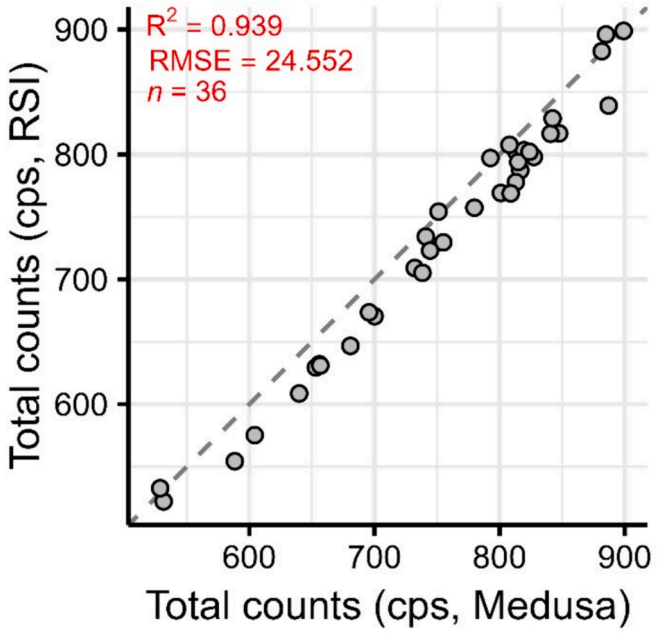

Fig. 8. Correlation between total gamma-ray counts measured by two different gamma-ray spectrometers (RapidMapper's Medusa MS-2000 vs. RSI RSX-1) at 36 reference sampling locations within the Booßen field. R^2: The coefficient of determination; RMSE: Root mean squared error; *n*: Number of count points. The gray and dashed line is the 1:1 line.

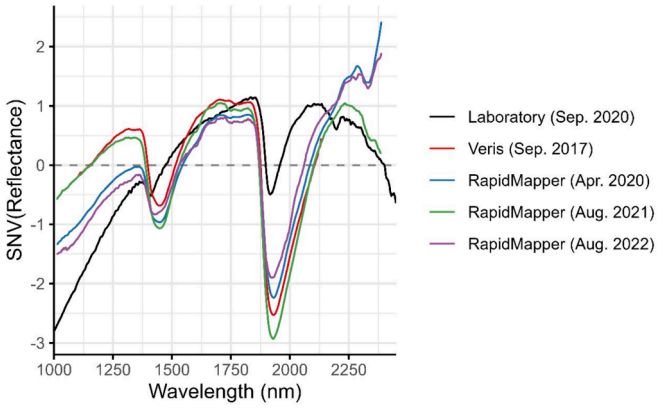

Fig. 9. The median NIR reflectance spectra obtained from laboratory and field measurements for the Booßen field. The field data includes measurements from RapidMapper across different years and Veris MSP in September 2017. All spectra have been normalized using the standard normal variate (SNV) technique.

soil moisture content, since O–H groups, including water absorb light at these wavebands (Viscarra Rossel and Behrens, 2010). NIR data from dried lab samples exhibits higher contrast, leading to better quality. Encouragingly, field-moist data collected with the RapidMapper NIR also produces valid spectra due to the similarity in spectral patterns with the lab data.

Although total reflectance values alone may not provide a definitive assessment of NIR data, we selected this variable as a representative of the data for our correlation analysis. As shown in Fig. 5, the total reflectance of the NIR lab spectra showed a very strong correlation with field data from the 2020 survey, a good correlation with the 2022 data, and a weaker correlation with the 2021 data. The RapidMapper NIR total reflectance data from 2020 and 2021 showed a higher correlation with the Veris MSP data (2017) compared to the 2022 data of RapidMapper Fig. 5.

This section compared NIR data from RapidMapper to those acquired by Veris MSP and laboratory measurements. While some similarities were observed, definitively assessing the data correspondence is challenging. Future works will involve developing soil property calibration models using this data, which may provide a more robust basis for comparison.

4. Conclusions

In this study, we introduced a newly developed multi-sensor platform (called RapidMapper) for topsoil mapping. The platform is currently equipped with a suite of four sensors, including NIR and gamma-ray spectroscopy as well as geoelectric and pH potentiometry sensors. To evaluate the functionalities of the platform, we conducted field mappings on various soils in Germany. Furthermore, for a thorough assessment of the platform's data quality, we selected two fields for in-depth analysis of RapidMapper's performance. Data quality was evaluated through a) an assessment of the general functionality for consistent mapping of various fields across Germany, b) a sensitivity assessment: the sensors response across different soil types was assessed, c) temporal consistency assessment: Verifying consistency of measurements on the same field over three years, d) similar sensors' comparison: Comparing ECa, gamma-ray and NIR data from the platform with other devices, and e) *in-situ* vs. laboratory measurement's comparison: Comparing field NIR data and laboratory measurements. The following conclusions can

be drawn from this research:

- The platform demonstrated consistent mapping capabilities across diverse fields in Germany.
- Sensor readings accurately reflected soil property variations in different soils.
- RapidMapper measurements exhibited high temporal consistency on the same field over multiple years.
- Electrical conductivity (EC) and gamma-ray measurements by RapidMapper showed strong agreement with those from other devices.
- Similarities were observed between the platform's *in-situ* NIR data and that obtained from laboratory measurements.
- The strong concordance between RapidMapper's data and that collected from other devices demonstrates the feasibility of merging data from diverse campaigns and instruments into a unified database. With respect to the wide range of pedological conditions that exist, a large database is needed to build a site-independent soil property model. Such a model is needed when site-specific calibrations are to be overcome.
- The RapidMapper's initial field tests yielded positive outcomes. The platform enables the operation of several soil sensors in parallel. However, the complexity of the system makes it error prone. In particular, using MS Windows as the operating system generates problems with the timing of commands and data transfer.
- More fields with diverse soil conditions need to be mapped by the platform and soil property calibration models need to be built with the data to generalize our observations and further test its performance.

CRediT authorship contribution statement

Hamed Tavakoli: Conceptualization, Data curation, Investigation, Methodology, Visualization, Writing – original draft. **José Correa:** Data curation, Formal analysis, Visualization, Writing – original draft. **Sebastian Vogel:** Methodology, Project administration, Supervision, Writing – review & editing. **Marcel Oertel:** Methodology, Software. **Marc Zimne:** Methodology, Visualization, Writing – review & editing. **Michael Heisig:** Software, Writing – review & editing. **Anatolij Harder:** Investigation, Methodology. **Robert Wruck:** Investigation, Methodology. **Stefan Pätzold:** Data curation, Investigation, Writing – review & editing. **Matthias Leenen:** Data curation, Investigation. **Robin Gebbers:** Conceptualization, Methodology, Project administration, Supervision, Writing – review & editing.

Declaration of competing interest

The authors declare that they have no known competing financial interests or personal relationships that could have appeared to influence the work reported in this paper.

Data availability

Data will be made available on request.

Acknowledgments

The authors would like to acknowledge the Federal Ministry of Education and Research (BMBF) of Germany for funding the I4S project (grant number 031B1069A), and the project partners: Ferdinand-Braun-Institute, Hahn-Schickard-Society, Technical University Munich, University of Bonn, Martin-Luther-University, University of Potsdam, ZALF, BAM, Geophilus GmbH, for their valuable contributions to the project. We warmly thank the efforts of all colleagues who contributed to the development of the RapidMapper platform.

Appendix A. Supplementary material

Supplementary data to this article can be found online at https://doi.org/10.1016/j.compag.2024.109443.

References

Adamchuk, V.I., Morgan, M.T., Ess, D.R., 1999. An automated sampling system for measuring soil pH. Transactions of the ASAE 42, 885–892.
Adamchuk, V.I., Viscarra Rossel, R.A., 2010. Development of On-the-Go Proximal Soil Sensor Systems. In: Viscarra Rossel, R.A., McBratney, A.B., Minasny, B. (Eds.), Proximal Soil Sensing. Springer, Netherlands, Dordrecht, pp. 15–28.
Allred, B., Daniels, J.J., Ehsani, M.R., 2008. Handbook of Agricultural Geophysics CRC Press.
Bönecke, E., Meyer, S., Vogel, S., Schröter, I., Gebbers, R., Kling, C., Kramer, E., Lück, K., Nagel, A., Philipp, G., Gerlach, F., Palme, S., Scheibe, D., Zieger, K., Rühlmann, J., 2021. Guidelines for precise lime management based on high-resolution soil pH, texture and SOM maps generated from proximal soil sensing data. Precis. Agric. 22, 493–523.
Gebbers, R., 2018. Proximal Soil Surveying and Monitoring Techniques. In: Stafford, J. (Ed.), Precision Agriculture for Sustainability. Burleigh Dodds Scientific Publishing, Cambridge, UK.
Gebbers, R., Adamchuk, V.I., 2010. Precision agriculture and food security. Science 327, 828–831.
Gebbers, R., Lück, E., Dabas, M., Domsch, H., 2009. Comparison of instruments for geoelectrical soil mapping at the field scale. Near Surf. Geophys. 7, 179–190.
Group, I.W., 2015. World reference base for soil resources 2014, update 2015. Food and Agriculture Organization of the United Nations - World Soil Resources Reports, Rome.
Hardie, M., 2020. Review of novel and emerging proximal soil moisture sensors for use in agriculture. Sensors 20, 6934.
Heggemann, T., Welp, G., Amelung, W., Angst, G., Franz, S.O., Koszinski, S., Schmidt, K., Pätzold, S., 2017. Proximal gamma-ray spectrometry for site-independent in situ prediction of soil texture on ten heterogeneous fields in Germany using support vector machines. Soil Tillage Res. 168, 99–109.
Hiemstra, P.H., Pebesma, E.J., Twenhöfel, C.J.W., Heuvelink, G.B.M., 2009. Real-time automatic interpolation of ambient gamma dose rates from the Dutch radioactivity monitoring network. Comput. Geosci. 35 (8), 1711–1721.
Hummel, J.W., Gaultney, L.D., Sudduth, K.A., 1996. Soil property sensing for site-specific crop management. Comput. Electron. Agric. 14, 121–136.
Federal Institute for Geosciences and Natural Resources (BGR), 2013. Soil overview map of the Federal Republic of Germany 1:1,000,000 with differentiation in land use (BÜK1000N V2.1), Hannover.
Javadi, S.H., Munnaf, M.A., Mouazen, A.M., 2021. Fusion of Vis-NIR and XRF spectra for estimation of key soil attributes. Geoderma 385, 114851.
Ji, W., Adamchuk, V.I., Chen, S., Mat Su, A.S., Ismail, A., Gan, Q., Shi, Z., Biswas, A., 2019. Simultaneous measurement of multiple soil properties through proximal sensor data fusion: A case study. Geoderma 341, 111–128.
Knödel, K., Krummel, H., Lange, G., 2005. Handbuch zur Erkundung des Untergrundes von Deponien und Altlasten, 2 ed. Springer, Berlin, Heidelberg, Berlin.
Kodaira, M., Shibusawa, S., 2013. Using a mobile real-time soil visible-near infrared sensor for high resolution soil property mapping. Geoderma 199, 64–79.
Kodaira, M., Shibusawa, S., 2020. Mobile proximal sensing with visible and near infrared spectroscopy for digital soil mapping. Soil Systems 4, 40.
Kuang, B., Mahmood, H.S., Quraishi, M.Z., Hoogmoed, W.B., Mouazen, A.M., van Henten, E.J., 2012. Chapter four - Sensing Soil Properties in the Laboratory, In Situ, and On-Line: A Review. In: Sparks, D.L. (Ed.), Advances in Agronomy. Academic Press, pp. 155–223.
La, W.-J., A. Sudduth, K., Kim, H.-J., Chung, S.-O., 2016. Fusion of spectral and electrochemical sensor data for estimating soil macronutrients. Trans. ASABE 59, 787–794.
Lueck, E., Ruehlmann, J., 2013. Resistivity mapping with GEOPHILUS ELECTRICUS — Information about lateral and vertical soil heterogeneity. Geoderma 199, 2–11.
Mahmood, H.S., Hoogmoed, W.B., van Henten, E.J., 2012. Sensor data fusion to predict multiple soil properties. Precis. Agric. 13, 628–645.
Mouazen, A.M., Maleki, M.R., Cockx, L., Van Meirvenne, M., Van Holm, L.H.J., Merckx, R., De Baerdemaeker, J., Ramon, H., 2009. Optimum three-point linkage set up for improving the quality of soil spectra and the accuracy of soil phosphorus measured using an on-line visible and near infrared sensor. Soil Tillage Res. 103, 144–152.
Mouazen, A.M., Alhwaimel, S.A., Kuang, B., Waine, T., 2014. Multiple on-line soil sensors and data fusion approach for delineation of water holding capacity zones for site specific irrigation. Soil Tillage Res. 143, 95–105.
Munnaf, M.A., Haesaert, G., Van Meirvenne, M., Mouazen, A.M., 2020. Chapter Five - Site-Specific Seeding Using Multi-Sensor and Data Fusion Techniques: A review. In: Sparks, D.L. (Ed.), Advances in Agronomy. Academic Press, pp. 241–323.
Nocita, M., Stevens, A., van Wesemael, B., Aitkenhead, M., Bachmann, M., Barthès, B., Ben Dor, E., Brown, D.J., Clairotte, M., Csorba, A., Dardenne, P., Demattê, J.A.M., Genot, V., Guerrero, C., Knadel, M., Montanarella, L., Noon, C., Ramirez-Lopez, L., Robertson, J., Sakai, H., Soriano-Disla, J.M., Shepherd, K.D., Stenberg, B., Towett, E. K., Vargas, R., Wetterlind, J., 2015. Chapter Four - Soil Spectroscopy: An Alternative to Wet Chemistry for Soil Monitoring. In: Sparks, D.L. (Ed.), Advances in Agronomy. Academic Press, pp. 139–159.

Pätzold, S., Leenen, M., Heggemann, T.W., 2020. Proximal mobile gamma spectrometry as tool for precision farming and field experimentation. Soil Systems 4 (2), 31.
Pebesma, E.J., 2004. Multivariable geostatistics in S: the gstat package. Comput. Geosci. 30, 683–691.
QGIS.org, 2023. QGIS Geographic Information System. QGIS Association.
Savitzky, A., Golay, M.J.E., 1964. Smoothing and differentiation of data by simplified least squares procedures. Anal. Chem. 36, 1627–1639.
Schmidinger, J., Schröter, I., Bönecke, E., Gebbers, R., Ruehlmann, J., Kramer, E., Mulder, V.L., Heuvelink, G.B.M., Vogel, S., 2024. Effect of training sample size, sampling design and prediction model on soil mapping with proximal sensing data for precision liming. Precis. Agric. 25, 1529–1555.
Schwalb-Willmann, J., 2024. basemaps: Accessing Spatial Basemaps in R. R Package Version 7.
Stenberg, B., Viscarra Rossel, R.A., Mouazen, A.M., Wetterlind, J., 2010. Chapter Five - Visible and Near Infrared Spectroscopy in Soil Science. In: Sparks, D.L. (Ed.), Advances in Agronomy. Academic Press, pp. 163–215.
Team, R.C., 2019. R: A language and environment for statistical computing. . R Foundation for Statistical Computing, Vienna, Austria.
Viscarra Rossel, R.A., Adamchuk, V.I., Sudduth, K.A., McKenzie, N.J., Lobsey, C., 2011. Chapter Five - Proximal Soil Sensing: An Effective Approach for Soil Measurements in Space and Time. In: Sparks, D.L. (Ed.), Advances in Agronomy. Academic Press, pp. 243–291.
Viscarra Rossel, R.A., Behrens, T., 2010. Using data mining to model and interpret soil diffuse reflectance spectra. Geoderma 158, 46–54.
Vogel, S., Bönecke, E., Kling, C., Kramer, E., Lück, K., Philipp, G., Rühlmann, J., Schröter, I., Gebbers, R., 2022. Direct prediction of site-specific lime requirement of arable fields using the base neutralizing capacity and a multi-sensor platform for on-the-go soil mapping. Precis. Agric. 23, 127–149.
Vonau, W., Decker, M., Enseleit, U., Gerlach, F., 2020. Is there still a need for the antimony electrode 100 years after its introduction as a pH sensor? J. Solid State Electrochem. 24, 3269–3277.
Wickham, H., Averick, M., Bryan, J., Chang, W., McGowan, L., François, R., Grolemund, G., Hayes, A., Henry, L., Hester, J., Kuhn, M., Pedersen, T., Miller, E., Bache, S., Müller, K., Ooms, J., Robinson, D., Seidel, D., Spinu, V., Takahashi, K., Vaughan, D., Wilke, C., Woo, K., Yutani, H., 2019. Welcome to the Tidyverse. Journal of Open Source Software 4, 1686.
Xu, X., Du, C., Ma, F., Shen, Y., Wu, K., Liang, D., Zhou, J., 2019b. Detection of soil organic matter from laser-induced breakdown spectroscopy (LIBS) and mid-infrared spectroscopy (FTIR-ATR) coupled with multivariate techniques. Geoderma 355, 113905.
Xu, D., Zhao, R., Li, S., Chen, S., Jiang, Q., Zhou, L., Shi, Z., 2019a. Multi-sensor fusion for the determination of several soil properties in the Yangtze River Delta, China. Eur. J. Soil Sci. 70, 162–173.
Zhang, Y., Hartemink, A.E., 2020. Data fusion of vis–NIR and PXRF spectra to predict soil physical and chemical properties. Eur. J. Soil Sci. 71, 316–333.